

Photoelectrochemical Reduction of CO₂ to Alcohols at CuO/CuFeO₂ Thin Film Electrode

Jiongliang Yuan^{1,*}, Liu Yang¹, Cunjiang Hao²

¹ Department of Environmental Science and Engineering, Beijing University of Chemical Technology, Beijing 100019, P. R. China

² School of Chinese Materia Medica, Tianjin University of Traditional Chinese Medicine, Tianjin 300193, P. R. China

*E-mail: yuanjiongliang@163.com.

Received: 6 March 2019 / Accepted: 17 May 2019 / Published: 31 July 2019

CuFeO₂/CuO thin film electrodes are fabricated by electrodeposition method in dimethyl sulfoxide. With the increase of deposition potential and annealing temperature, the peak intensity of both CuO(111) and CuFeO₂(101) becomes stronger. The resulted thin film electrodes exhibit high absorbance in visible light range. The photoelectrocatalytic performance of CuFeO₂/CuO thin film electrodes for CO₂ reduction is examined. At the applied potential between -0.50 to -0.80 V (vs. saturated calomel electrode), CO₂ can be reduced to methanol and ethanol. The highest concentration of ethanol occurs at the applied potential of -0.63 V, whereas that of methanol occurs at -0.70 V. There is a strong relationship between Cu/Fe molar ratio on the thin film electrode surface and ethanol concentration, and ethanol concentration increases with the decrease of the Cu/Fe molar ratio of the thin film surface.

Keywords: CuO/CuFeO₂ thin film electrode, photoelectrochemical reduction, carbon dioxide, methanol, ethanol.

1. INTRODUCTION

The depletion of fossil fuel produces a vast amount of CO₂ emission which causes the global warming. Producing carbon fuels with a reduced CO₂ emission profile has attracted intensive attention [1]. The conversion of CO₂ to carbon fuels can be implemented through various routes, eg. thermochemical, biochemical, photo- and/or electrochemical reactions [2-6]. Among which, owing to harnessing the solar energy, photochemical/ photoelectrochemical routes show favourable prospects [3]. Such carbon fuels as carbon monoxide, methane, methanol and ethanol can be obtained by photochemical/ photoelectrochemical conversion [3,7-9]. Since both methanol and ethanol are promising liquid fuels in the view of high energy density, convenient storage and

transportation, the reduction of CO₂ to methanol and ethanol is promising [10,11]. With the catalysis of semiconductors such as TiO₂ and InTaO₄, CO₂ can be photochemically reduced to methanol [12-15]. On the g-C₃N₄/ZIF-67 composite photocatalyst, CO₂ can be converted into ethanol [16]. However, the photocatalysts usually exhibit low activity and poor selectivity. Photoelectrocatalysis can promote the separation efficiency of electrons and holes, the photocatalytic activity and selectivity can therefore be increased pronouncedly. At CuInS₂ thin film photocathode, CO₂ can be reduced to methanol with faradaic efficiency up to 97% [17]. Using the Cu-In/CuInS₂ composite thin film as the photocathode, CO₂ can be photoelectrochemically reduced to methanol and ethanol with ethanol as the major product [18]. However, up to date, developing the high-efficiency and low-cost photoelectrodes has still been a huge challenge.

CuFeO₂ with the delafossite structure has a suitable band gap that is well-matched to the solar spectrum, high stability and environmental friendliness [19]; more important, it exhibits good optoelectric conversion performance in visible light region. It has been used for photoelectrochemical reduction of water to hydrogen and reduction of CO₂ to formate [20-24]. In addition, it has been reported that CO₂ is reduced to methanol at CuO photoelectrode with low activity [25]. In this study, CuO/CuFeO₂ thin film electrodes are fabricated by electrodeposition method, and using the resulted CuO/CuFeO₂ thin film electrodes as the photocathodes, CO₂ is reduced to methanol and ethanol with high activity.

2. EXPERIMENTAL

2.1. Fabrication of CuO/CuFeO₂ thin film electrodes

The electrodeposition of CuO/CuFeO₂ thin film electrodes was conducted by a CHI660D electrochemical workstation (Shanghai Chenhua Instrument Co. Ltd., Shanghai, P. R. China). A standard three-electrode arrangement was used; F-doped SnO₂ (FTO) conductive glass substrate, the platinum foil and the saturated calomel electrode (SCE) were used as the working electrode, counter electrode and reference electrode, respectively. The deposition bath containing 3 mM Cu(NO₃)₂, 9 mM Fe(NO₃)₃ and 150 mM NaClO₄ in dimethyl sulfoxide (DMSO) was employed in the electrodeposition of CuO/CuFeO₂ thin film electrodes. Electrodeposition was conducted at -0.45, -0.50, -0.60, -0.70 and -0.80 V (vs. SCE) for 1.5 h at 25 °C. After electrodeposition, the thin films were annealed at 540, 560, 580 and 600°C for 30 min in atmospheric air, respectively.

The crystal structure of CuO/CuFeO₂ thin films was determined by X-ray diffractometry (XRD, D/MAX2500, Rigaku, Japan). The Raman spectra of the thin films were collected on confocal micro Raman spectrometer (inVia, Renishaw). The x-ray photoelectron spectra (XPS) were collected on ESCALAB 250 (ThermoFisher Scientific, USA) equipped with x-ray source of twin anode Al K α 300 W. All binding energies were calibrated to C1s at 284.6 eV. The molar ratio of Cu/Fe on thin film surface was obtained by XPS measurement. The UV-Vis spectra of CuO/CuFeO₂ thin film electrodes were measured by UV-vis-NIR spectrophotometer (UV-3600, Shimadzu, Japan).

2.2. Photoelectrochemical reduction of CO₂

The photoelectrochemical reduction of CO₂ was performed on the electrochemistry work station CHI660E with 0.1 M acetate buffer solution (50 mL) containing 10 mM pyridine. Five runs were done for one experiment. A standard three-electrode cell was used with CuO/CuFeO₂ thin film electrode (1×2 cm²) as the working electrode, graphite sheet (10 cm²) as the counter electrode and SCE as the reference electrode. The visible light irradiation was emitted from xenon lamp (AULTT, Beijing, P. R. China) with the calibrated irradiation intensity of 100 mW/cm² on the thin film electrode.

All photoelectrochemical experiments were performed at 25 °C and ambient pressure. Before each experiment, the electrolyte had been purged with CO₂ for 30 min. CO₂ gas was continuously aerated at the flow rate of 60 ml/min during the electrolysis process. CO₂ reduction experiments were conducted for 1.5 h. Liquid product was analyzed using a gas chromatography-mass spectroscopy (GC-MS, Trace 1300-ISQ, ThermoFisher Scientific). Methanol and ethanol concentration was measured by a gas chromatography (GC 2014C, Shimadzu, Japan) with a DB-Wax (30 m × 0.53 mm × 3.00 μm, Agilent Technologies). The injector temperature was held at 200 °C, the oven temperature was elevated from 50 to 200 °C at a rate of 5 °C/min, and the detector temperature was kept at 230 °C. During a typical run, only peaks related to the elution of methanol, ethanol and pyridine were observed.

Linear scanning voltammetric measurement was conducted in the above three-electrode cell, and scanning potential was set from 0 to -1 V (vs. SCE) at 0.005 V/s. The photocurrent density was recorded with 0.1 M acetate buffer solution (50 mL) containing 10 mM pyridine. The calibrated irradiation intensity on the thin film electrode is 100 mW/cm².

3. RESULTS AND DISCUSSION

3.1. Fabrication of CuO/CuFeO₂ thin film electrodes

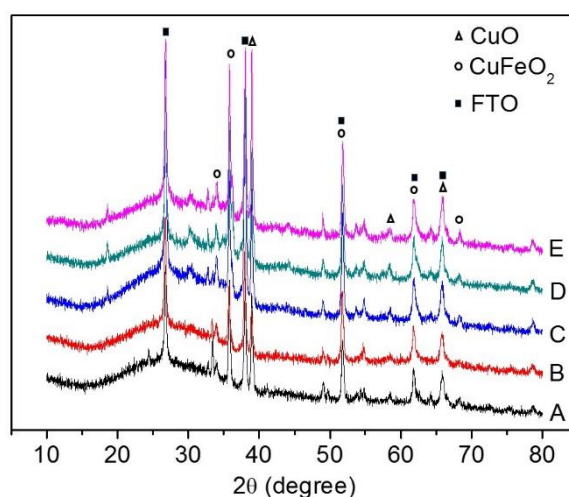


Figure 1. XRD patterns for CuO/CuFeO₂ thin films deposited at various potential for 1.5 h and annealed at 580 °C for 30min. A. -0.45 V, B. -0.50 V, C. -0.60 V, D. -0.70 V, E. -0.80 V.

The XRD patterns for CuO/CuFeO₂ thin films deposited at various potential are shown in Fig. 1. At the potential from -0.45 to -0.80 V, CuO/CuFeO₂ thin films can be obtained. With the increase of deposition potential, the peak intensity of both CuO (111) ($2\theta=38.7^\circ$) and CuFeO₂ (101) ($2\theta=35.8^\circ$) becomes stronger. No peaks for other oxides (e.g., CuFeO_{2+ δ} , CuFe₂O₄, or Fe₃O₄) are observed. At the potential negative to -0.60 V, CuFeO₂ (012) ($2\theta=36.1^\circ$) peak occurs.

Choi *et al.* have reported the electrodeposition of CuFeO₂ thin films in DMSO solution at the potential of -0.3 V vs Ag/AgCl (4 M KCl) reference, and the crystallinity of CuFeO₂ is very poor [22]. In contrast, in our study, the deposition potential is more negative, thus CuFeO₂ of higher crystallinity is obtained.

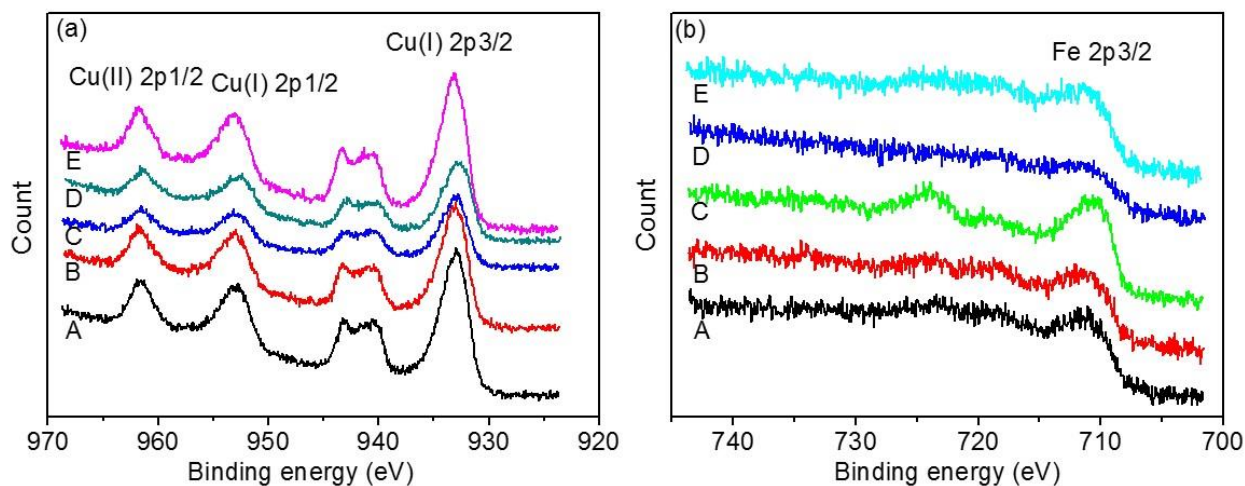


Figure 2. XPS characteristics of Cu2p for CuO/CuFeO₂ thin film electrodes deposited at various potential for 1.5 h and annealed at 580 °C for 30 min. A.-0.45 V, B. -0.50 V, C. -0.60 V, D. -0.70 V, E. -0.80 V.

XPS characteristics of Cu2p and Fe2p for CuO/CuFeO₂ thin film electrodes deposited at various potential are shown in Fig. 2. It can be seen that both Cu(I) and Cu(II) exist, corresponding to CuFeO₂ and CuO; Fe2p_{3/2} peaks locate at ca. 710.5 eV, which were assigned to Fe(III) [26]. XRD and XPS results demonstrate that the co-electrodeposition of Cu(II) and Fe(III) and subsequent oxidative annealing create CuO and CuFeO₂ bicrystallines.

Table 1. Chemical composition of CuO/CuFeO₂ thin film surface at various deposition potential for 1.5 h. ^a

Deposition potential (V)	-0.45	-0.50	-0.60	-0.70	-0.80
Molar ratio of Cu/Fe on thin film surface	7.03	5.46	2.48	3.02	3.65

^a CuO/CuFeO₂ thin films were annealed at 580 °C for 30 min.

The deposition potential of CuO/CuFeO₂ thin films has a significant effect on Cu/Fe molar ratio of thin film surface (Table 1). With the increase of deposition potential from -0.45 to -0.60 V, the molar ratio of Cu/Fe on thin film surface decreases; however, the molar ratio of Cu/Fe increases when the deposition potential is negative to -0.60 V. It indicates that the molar ratio of CuO to CuFeO₂ of thin film surface is the lowest at the deposition potential of -0.60 V.

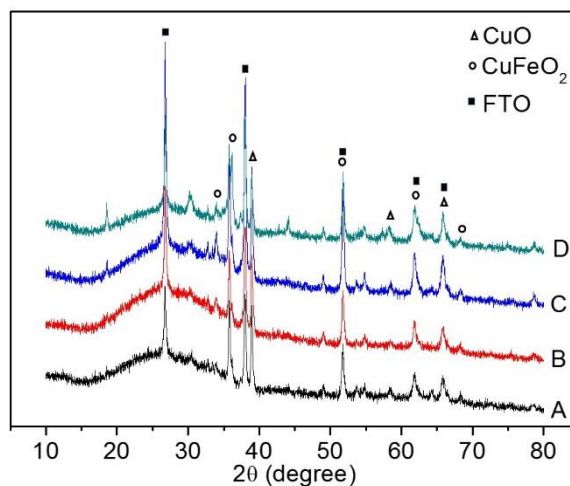


Figure 3. XRD patterns for CuO/CuFeO₂ thin films deposited at -0.60 V for 1.5 h and annealed at various temperature for 30 min. A. 540 °C, B. 560 °C, C. 580 °C, D. 600 °C.

The effect of annealing temperature on the structure of CuO/CuFeO₂ thin films deposited at -0.60 V is shown in Fig. 3. With the increase of annealing temperature, the peak intensity of both CuO and CuFeO₂ becomes stronger, showing that their crystallinity increases. However, the sample annealed at 600 °C shows lower intensity of CuO and CuFeO₂ peaks, and the peaks of CuFeO₂ (012) ($2\theta=36.1^\circ$) and (015) ($2\theta=44.1^\circ$) occur.

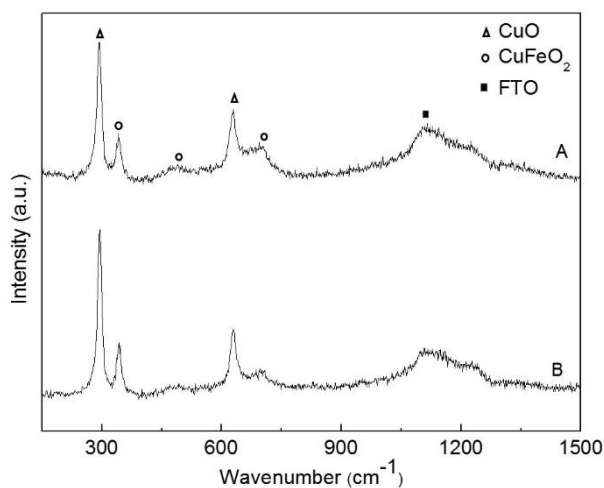


Figure 4. Raman spectra for CuO/CuFeO₂ thin films deposited at various potential for 1.5 h and annealed at 580 °C for 30 min. A. -0.45 V, B. -0.60 V.

The Raman spectra of CuO/CuFeO₂ thin films deposited at -0.45 and -0.60 V are shown in Fig. 4. Both samples exhibit similar spectral features. The peaks at 295 and 628 cm⁻¹ are corresponding to CuO, and those at 348, 505 and 684 cm⁻¹ are assigned to delafossite CuFeO₂, indicating that both CuO and CuFeO₂ phases exist in those thin films [27]. No Fe₂O₃ phase is detected in CuO/CuFeO₂ thin films.

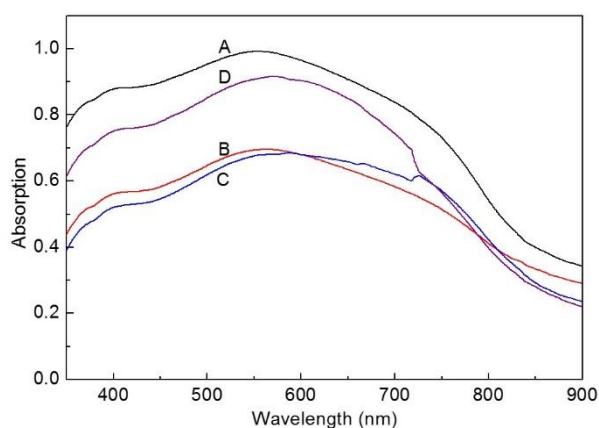


Figure 5. UV-vis spectra for CuO/CuFeO₂ thin films deposited at various potential for 1.5 h and annealed at 580 °C for 30 min. A-0.45 V, B. -0.50 V, C. -0.60 V, D. -0.80 V.

Both CuO and CuFeO₂ can utilize visible light sufficiently for their narrow energy band gap [28-30]. The UV-vis spectra of CuO/CuFeO₂ thin films deposited at various potential are presented in Fig. 5. All samples exhibit high absorbance in the range from 350 to 750 nm, and the electrodeposition potential has a significant effect on the absorbance. The thin films deposited at -0.45 and -0.80 V show higher adsorption.

3.2. Photoelectrochemical reduction of CO₂

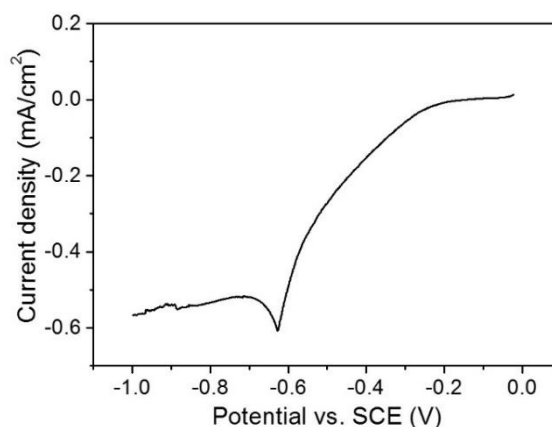


Figure 6. Voltammetric behavior of the illuminated CuO/CuFeO₂ thin film electrode in CO₂-saturated acetate buffer solution (0.1 M) containing 10 mM pyridine. CuO/CuFeO₂ thin film electrode was deposited at -0.60 V for 1.5 h and annealed at 580 °C. The calibrated irradiation intensity of visible light on the thin film electrode is 100 mW/cm². The scanning potential was set from 0 to -1 V at 0.005 V/s.

The voltammetric behavior of the illuminated CuO/CuFeO₂ thin film electrode is studied in CO₂-saturated acetate buffer solution (0.1 M) containing 10 mM pyridine (Fig. 6). A distinct cathodic current appears at -0.63 V, indicating that CO₂ is reduced. The liquid products in CO₂ photoelectrochemical reduction at -0.63 V are methanol and ethanol detected by GC-MS, and no other liquid products are detected. Park et al. have reported that CO₂ is photoelectrochemically reduced to formate at CuFeO₂/CuO photocathode in a CO₂-purged 0.1 M bicarbonate electrolyte under irradiation of AM 1.5G (100 mW/cm²) [23]. The difference in products is originated from the different surface composition of the photocathode and the different electrolyte [23].

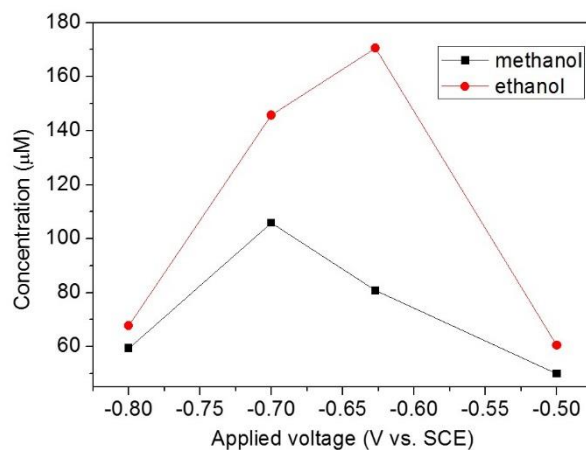


Figure 7. Concentration of methanol and ethanol at various applied voltage in CO₂ photoelectrochemical reduction. CuO/CuFeO₂ thin film electrode was deposited at -0.60 V for 1.5 h and annealed at 580 °C for 30 min. Photoelectrochemical reduction of CO₂ was performed in 0.1 M acetate buffer solution (50 mL) containing 10 mM pyridine for 1.5 h. The surface area of CuO/CuFeO₂ thin film electrode is 2 cm². The calibrated irradiation intensity of visible light on the thin film electrode is 100 mW/cm².

The effect of applied voltage in CO₂ photoelectrochemical reduction on the product concentration is presented in Fig. 7. It can be observed that methanol and ethanol are obtained at the applied voltage from -0.50 to -0.80 V. The highest concentration of methanol appears at -0.70 V, whereas that of ethanol occurs at -0.63 V, which is the same as the peak potential in Fig. 6. Due to hydrogen evolution reaction, the concentration of both products decreases from -0.70 to -0.80 V.

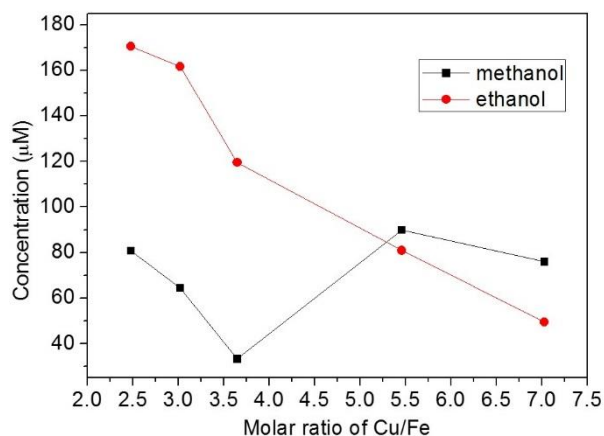


Figure 8. Concentration of methanol and ethanol at various molar ratio of Cu/Fe. CuO/CuFeO₂ thin film electrode was annealed at 580 °C for 30 min. Photoelectrochemical reduction of CO₂ was performed in 0.1 M acetate buffer solution (50 mL) containing 10 mM pyridine for 1.5 h. The surface area of CuO/CuFeO₂ thin film electrode is 2 cm². The calibrated irradiation intensity of visible light on the thin film electrode is 100 mW/cm².

The molar ratio of Cu/Fe of thin film surface has a significant impact on the yield of the products (Fig. 8). Ethanol concentration increases with the decrease of Cu/Fe molar ratio of thin film surface, and it reaches the maximum at the molar ratio of 2.48. It indicates that lower molar ratio of CuO/CuFeO₂ on the thin film surface promotes the formation of ethanol. The highest concentration of methanol occurs at Cu/Fe molar ratio of 5.46.

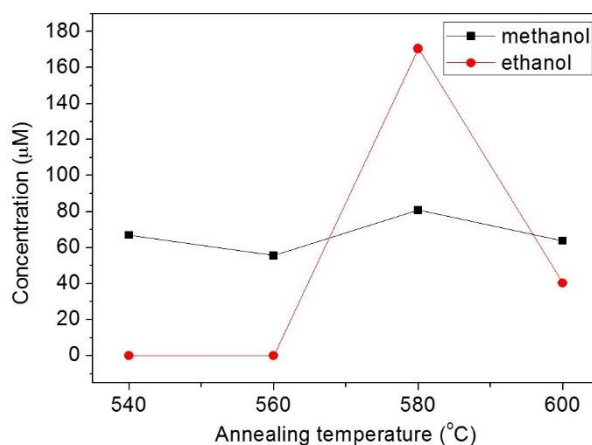


Figure 9. Concentration of methanol and ethanol at CuO/CuFeO₂ thin film electrodes deposited at -0.60 V for 1.5 h and annealed at various temperature for 30 min. Photoelectrochemical reduction of CO₂ was performed in 0.1 M acetate buffer solution (50 mL) containing 10 mM pyridine for 1.5 h. The surface area of CuO/CuFeO₂ thin film electrode is 2 cm². The calibrated irradiation intensity of visible light on the thin film electrode is 100 mW/cm².

The effect of annealing temperature of thin film electrodes on product concentration is shown in Fig. 9. With the increase of annealing temperature, ethanol concentration increases, and the highest concentration occurs at annealing temperature of 580 °C, then ethanol concentration decreases. It might

be due to the highest crystallinity of CuO and CuFeO₂ at 580 °C as shown in Fig. 3. In contrast, methanol concentration varies a little.

4. CONCLUSIONS

CuFeO₂/CuO thin film electrodes are fabricated by potentiostatic deposition in DMSO and they exhibit high absorbance in visible light range. XRD and Raman spectrum results show that both CuO and CuFeO₂ phases exist. With the increase of deposition potential, the peak intensity of both CuO(111) and CuFeO₂(101) becomes stronger. At CuFeO₂/CuO thin film electrodes, CO₂ can be photoelectrochemically reduced to methanol and ethanol. The highest concentration of ethanol occurs at the applied voltage of -0.63 V, whereas that of methanol occurs at -0.70 V. Higher molar ratio of CuFeO₂/CuO on the thin film surface promotes the formation of ethanol. With the increase of annealing temperature, ethanol yield increases, and the highest concentration occurs at annealing temperature of 580 °C.

ACKNOWLEDGMENTS

We gratefully acknowledge National Natural Sciences Foundation of China (Grant No. 20676010) for financial support.

References

1. F. Zeman and M. Castaldi, *Environ. Sci. Technol.*, 42 (2008) 2723.
2. S. K. Kuk, R. K. Singh, D. H. Nam, R. Singh, J. K. Lee and C. B. Park, *Angew. Chem. Int. Ed.*, 56 (2017) 3827.
3. B. Kumar, M. Llorente, J. Froehlich, T. Dang, A. Sathrum and C. P. Kubiak, *Annu. Rev. Phys. Chem.*, 63 (2012) 541.
4. Q. Liu, L. Wu, R. Jackstell and M. Beller, *Nat. Commun.*, 6 (2015) 5933.
5. Y. Ma, X. Wang, Y. Jia, X. Chen, H. Han and C. Li, *Chem. Rev.*, 114 (2014) 9987.
6. K. K. Sakimoto, A. B. Wong and P. Yang, *Science*, 351 (2016) 74.
7. D. D. Zhu, J. L. Liu and S. Z. Qiao, *Adv. Mater.*, 28 (2016) 3423.
8. L. Zhang, Z. J. Zhao and J. Gong, *Angew. Chem., Int. Ed.*, 56 (2017) 11326.
9. R. Kortlever, J. Shen, K. J. P. Schouten, F. Calle-Vallejo and M. T. M. Koper, *J. Phys. Chem. Lett.*, 6 (2015) 4073.
10. J. Chang, L. Feng, K. Jiang, H. Xue, W. B. Cai, C. Liu and W. Xing, *J. Mater. Chem. A*, 4 (2016) 18607.
11. W. Huang, X. Y. Ma, H. Wang, R. Feng, J. Zhou, P. N. Duchesne, P. Zhang, F. Chen, N. Han, F. Zhao, J. Zhou, W. B. Cai and Y. Li, *Adv. Mater.*, 29 (2017) 1703057.
12. J. C.-S. Wu, H.-M. Lin and C.-L. Lai, *Appl. Catal. A: Gen.*, 296 (2005) 194.
13. I.-H. Tseng and J.C.-S. Wu, *Catal. Today*, 97 (2004) 113.
14. P.-W. Pan and Y.-W. Chen, *Catal. Commun.*, 8 (2007) 1546.
15. C. W. Tsai, H. M. Chen, R.-S. Liu, K. Asakura and T. Chan, *J. Phys. Chem. C*, 115 (2011) 10180.
16. Y. Meng, L. Zhang and H. Jiu, *Mat. Sci. Semicon. Proc.*, 95 (2019) 35.
17. J. Yuan and C. Hao, *Sol. Energ. Mat. Sol. C*, 108 (2013) 170.
18. C. An, J. Yuan and J. Zhu, *J. Electrochem. Soc.*, 165 (2018) H1066.
19. Y. Jin and G. Chumanov, *RSC Adv.*, 6 (2016) 26392.

20. M. S. Prevot, N. Guijarro and K. Sivula, *ChemSusChem*, 8 (2015) 1359.
21. J. Gu, A. Wuttig, J. W. Krizan, Y. Hu, Z. M. Detweiler, R.J. Cava and A.B. Bocarsly, *J. Phys. Chem. C*, 117 (2013) 12415.
22. C. G. Read, Y. Park and K.-S. Choi, *J. Phys. Chem. Lett.*, 3 (2012) 1872.
23. U. Kang, S. K. Choi, D. J. Ham, S.M. Ji, W. Choi, D.S. Han, A. Abdel-Wahab and H. Park, *Energy Environ. Sci.*, 8 (2015) 2638.
24. M. S. Prevot, Y. Li, N. Guijarro and K. Sivula, *J. Mater. Chem. A*, 4 (2016) 3018.
25. P. Li, J. Xu, H. Jing, C. Wu, H. Peng, J. Lu and H. Yin, *Appl. Catal. B: Environ.*, 156-157 (2014) 134.
26. A. Bak, W. Choi and H. Park, *Appl. Catal. B: Environ.*, 110 (2011) 207.
27. M. A. Sarabia , S. D. Rojas, Z. López-Cabaña , R. Villalba, G. González and A. L. Cabrera, *J. Phys. Chem. Solids*, 98 (2016) 271.
28. M. Lai, S. Mubeen, N. Chartuprayoon, A. Mulchandani, M. A. Deshusses and N. V. Myung, *Nanotechnology*, 21 (2010) 295601.
29. C. G. Read, Y. Park and K. S. Choi, *J. Phys. Chem. Lett.*, 3 (2012) 1872.
30. J. Gu, A. Wuttig, J. W. Krizan, Y. A. Hu, Z. M. Detweiler, R. J. Cava and A. B. Bocarsly, *J. Phys. Chem. C*, 117 (2013) 12415.

© 2019 The Authors. Published by ESG (www.electrochemsci.org). This article is an open access article distributed under the terms and conditions of the Creative Commons Attribution license (<http://creativecommons.org/licenses/by/4.0/>).